CHEMISTRY OF MATERIALS

ARTICLE

pubs.acs.org/cm

Organosilane-Assisted Transformation from Core−Shell to Yolk−Shell Nanocomposites

Yan Yang,[†,‡] Jian Liu,[†,§] Xiaobo Li,[†,‡] Xiao Liu,[†,‡] and Qihua Yang*[,†]

[†]State Key Laboratory of Catalysis, Dalian Institute of Chemical Physics, Chinese Academy of Sciences, 457 Zhongshan Road, Dalian 116023, China

[‡]Graduate School of the Chinese Academy of Sciences, Beijing 100049, China

[§]ARC Centre of Excellence for Functional Nanomaterials, Australian Institute for Bioengineering and Nanotechnology, The University of Queensland, Brisbane QLD 4072, Australia

Supporting Information

ABSTRACT: In this paper, we present the synthesis of yolk−shell nanocomposites (NCs) with moveable cores (Fe_3O_4, Au nanoparticles (NPs)) and functionalized organosilica mesoporous shells by an organosilane-assisted etching approach for the first time. This synthesis method is facile, general, and rapid. By adding organosilanes such as 1, 2-bis(trimethoxysilyl)ethane (BTME) and 1,4-bis(triethoxysilyl)benzene (BTEB) into the synthetic medium of NPs@silica (Fe_3O_4 and Au NPs) core−shell NCs, the organosilica species deposit on the surface of the core−shell NCs, while the initial silica shells can be subsequently dissolved to form the yolk−shell NCs. The formation of such yolk−shell NCs can be reasonably explained by a novel organosilane-assisted etching mechanism based on the results of FT-IR and ^{29}Si NMR spectroscopy. The yolk−shell NCs with Au cores exhibit much higher catalytic activity than the Au@silica core−shell NCs for the catalytic reduction of *o*-nitroaniline, probably due to the higher accessibility of the Au active sites in the yolk−shell NCs.

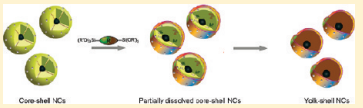

KEYWORDS: moveable cores, mesoporous shells, one-pot method, organosilane-assisted etching mechanism

1. INTRODUCTION

Recently, hollow nanostructures with moveable nanoparticles (NPs) as cores, so-called yolk−shell or rattle-type nanocomposites (NCs), have attracted great research interest because of their unique properties[1−8] and potential applications in the fields of catalysis,[9−12] lithium-ion batteries, and nanomedicine.[13−15] In comparison to the conventional structures that NPs embedded in supports, yolk−shell structures have the following advantages: (1) The outer shell can hinder the aggregation of neighboring particles, even under harsh reaction conditions.[16−18] (2) The moveable cores can afford more exposed active sites, which in turn provide much more effective interaction with the guest molecules, such as the reactants for catalysis.[19,20] (3) The interstitial hollow space can allow high loading space for functional molecules such as drugs.[21−24]

Several approaches have been developed for the synthesis of yolk−shell NCs,[25−29] such as soft template,[23,30,31] ship-in-bottle,[32] Kirkendall effect,[33] galvanic replacement,[34,35] and inside-out Ostwald ripening process.[36,37] Although some progress in the synthesis of yolk−shell NCs has been achieved, most of the methods mentioned above are complex and only work on samples with particular compositions and structures. An alternative way to produce yolk−shell NCs is a template-assisted selective etching approach. In this method, the presynthesized core materials are coated with a layer or double layers of different materials and then the middle layer of the double shells or the partial cores or shells of the core−shell materials can be selectively removed by dissolution with a solvent or via calcination. A series of yolk−shell NCs with different compositions of cores and shells have been fabricated through template-assisted selective etching method, such as metal NPs@polymer,[38−40] NPs@metal oxides,[41] NPs@silica,[42−46] and NPs@carbon.[47] However, this synthetic procedure is multistep and complex. Moreover, the variation of the compositions of the shells is difficult and thus limited. Therefore, a highly efficient and general way to produce yolk−shell NCs with tunable shell compositions is still a great challenge.

Herein, we report a facile organosilane-assisted etching method for the formation of yolk−shell NCs with metal oxides or metal NPs core materials such as Fe_3O_4 and Au NPs and tunable functionalized mesoporous shells in a one-pot medium. After the addition of organosilane precursors into a synthetic medium of NPs@silica (Fe_3O_4 and Au NPs) core−shell NCs, the formation of the outer mesoporous organosilica shells and dissolution of the inner mesoporous silica shells occur at the same time, which results in the evolution from core−shell to yolk−shell NCs. The whole process from the presynthesized Fe_3O_4 NPs to yolk−shell NCs only takes 3 h under the typical condition (BTME as organosilane). Compared with the selectively etching method, this strategy has the following advantages: (1) It is facial and simple through a one-pot medium. (2) The shell structure can be tunable with the aid of different kinds of surfactants. (3) The shell could be easily functionalized by varying the organosilane type.

Received: April 25, 2011
Revised: July 5, 2011
Published: July 20, 2011

Scheme 1. Illustration of Synthesis Procedure for the Yolk−Shell NCs with Organosilica-Functionalized Mesoporous Shells and Movable NPs as Cores

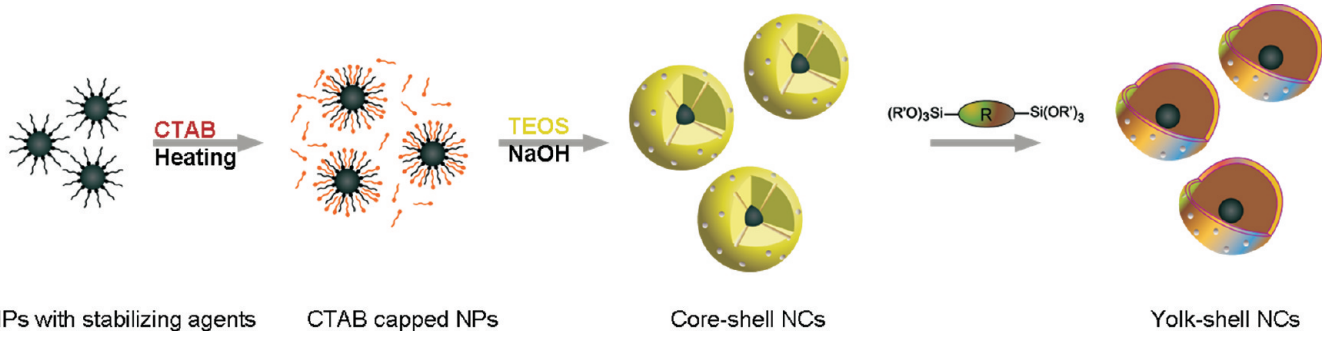

The formation mechanism was proposed by monitoring the synthetic process with TEM, XRD, nitrogen sorption, ^{29}Si NMR, and FT-IR characterizations. The yolk−shell NCs with Au cores can remarkably enhance the catalytic activity of Au NPs toward the catalytic reduction of *o*-nitroaniline compared to Au@SiO_2 core−shell NCs.

2. EXPERIMENTAL SECTION

2.1. Chemicals and Reagents. All materials were of analytical grade and used as received without any further purification. 1,2-Bis(trimethoxysilyl)ethane (BTME) and cetyltrimethylammonium bromide (CTAB) were purchased from Sigma-Aldrich Company Ltd. (USA). Fluorocarbon surfactant, FC-4, was bought from Yick Vic Chemicals (Hong Kong). 1,4-Bis(triethoxysilyl)benzene (BTEB) was purchased from ABCR GmbH & Co. KG (Germany). Tetramethoxysilane (TMOS) was obtained from Nanjing Shuguang Chemical Group (China). Other reagents were purchased from Shanghai Chemical Reagent, Inc. of the Chinese Medicine Group.

2.2.1. Synthesis of Core−Shell NCs (Fe_3O_4@SiO_2 Core−Shell NCs) and Yolk−Shell NCs (YS-60 and YS-60-FC4) with Fe_3O_4 Cores. A total of 0.3 mL of Fe_3O_4 NPs (particle size of ∼17 nm) capped with oleic acid[48] dispersed in chloroform (15 mg/mL) was added into 5 mL of aqueous solution containing 0.1 g of CTAB. After vigorous stirring of the resulted solution, a homogeneous oil-in-water microemulsion was obtained. Heating at 60 °C for 10 min induced the evaporation of chloroform in the solution, which generated aqueous-phase dispersed NPs. Then 350 μL of NaOH solution (2.0 M), 0.63 g of tetraethylorthosilicate (0.11 mmol) was successively added to the diluted aqueous solution containing the magnetite NPs under vigorous stirring, and the synthetic medium was kept for 2 h at 80 °C. The obtained materials were denoted as Fe_3O_4@SiO_2 core−shell NCs. For the synthesis of yolk−shell NCs, 60 g of water was added into the above solution. After the temperature of the mixture reaches to 80 °C, 360 μL BTME in ethanol solution (2 mL) was added. One hour later, the light brown product was collected by filtration and dried at room temperature. To remove the surfactant, the as-synthesized materials (1 g) were dispersed in a solution of 80 mg ammonium nitrate and 120 mL ethanol (95%) solution, and the mixture was heated at 60 °C for 30 min. The material after centrifugation and washing with ethanol was denoted as YS-60. YS-60-FC4 was also prepared using similar method to YS-60 with the exception that the aqueous solution (60 g) with 0.04 g of FC4, 0.08 g CTAB, and 600 μL $NH_3.H_2O$ (25 wt %) was added into the synthetic medium instead of 60 g water before the addition of BTME.

2.2.2. Comparable Experiments Using Other Organosilane Precursors. A total of 600 μL TEOS and 400 μL TMOS were also used instead of BTME in a similar way without any other change of the synthetic medium for the YS-60. For the yolk−shell sample synthesized with BTEB, not only 60 g water but also 24 mL ethanol (95%) were added into the synthetic medium of the Fe_3O_4@SiO_2 core−shell NCs before the addition of BTEB (520 μL) in ethanol solution (2 mL). The following processes were the same as that for the sample YS-60.

2.2.3. Synthesis of Core−Shell NCs (Au@SiO_2 Core−Shell NCs) and Yolk−Shell NCs (YS-Au-FC4) with Au Cores. Au@SiO_2 core−shell NCs and YS-Au-FC4 were prepared using similar method to Fe_3O_4@SiO_2 core−shell NCs and YS-60-FC4, except that Au NPs (∼6 nm) capped with oleylamine[49] in chloroform were used as starting core material.

2.2.4. Catalytic Reduction of o-NA. The catalyst (Au, 36.5 μmol) was added into freshly prepared $NaBH_4$ aqueous solution (2.0 mL, 1.2 M), and the mixture was stirred for 30 min at room temperature before the addition of the substrate. *o*-NA aqueous solution (6.0 mL, 5.0×10^{-3} M) was added, and the resulting mixture was stirred at room temperature until the yellow solution became colorless. The reaction progress was monitored by taking a small portion of the reaction mixture at a specified time. The solid catalysts were removed with a filter syringe and the obtained liquid was analyzed by UV−vis to monitor the conversation of the *o*-NA. The UV−vis peaks at 412 and 282 nm are characteristic of *o*-NA.[19] As the reaction proceeded, the peak at 412 nm disappeared, while the yellow solution became colorless. YS-Au-FC4 and Au@silica core−shell NCs were tested with the same amount of Au under otherwise the same conditions.

2.3. Characterization. X-ray powder diffraction (XRD) patterns were recorded on a Rigaku D/Max 3400 powder diffraction system using Cu Kα radiation (λ = 0.1541 nm). The nitrogen sorption experiments were performed at 77 K using a Micromeritrics ASAP 2020. Samples were degassed at 120 °C for 5 h prior to the measurements. BET surface area was calculated from the adsorption data in the relative pressure P/P_0 range from 0.04 to 0.2. Pore size distributions were determined from the adsorption branches using the Barret−Joyner−Halenda (BJH) method. Pore volume was estimated at the relative pressure P/P_0 of 0.99. Transmission electron microscopy (TEM) was performed using a FEI Tecnai G^2 Spirit at an acceleration voltage of 120 kV. The magnetization curve was measured at room temperature under a varying magnetic field with VSM. FT-IR spectra were collected with a Nicolet Nexus 470 IR spectrometer with KBr pellet. UV−vis spectra were collected with a Shimadazu UV-2550 spectrometer. Solid-state ^{29}Si (79.4 MHz) cross-polarization magic-angle-spinning (CP-MAS) NMR were obtained on a Bruker DRX-400 spectrometer equipped with a magic-angle-spin probe in a 4-mm ZrO_2 rotor using tetramethylsilane as reference. The experimental parameters are as follows: For ^{29}Si CP-MAS NMR experiments, 4-kHz spin rate, 3-s pulse delay, and 500 scans.

3. RESULTS AND DISCUSSION

3.1. Synthesis and Characterizations of Yolk−Shell NCs with Magnetic Cores. The typical procedure for the preparation

dx.doi.org/10.1021/cm201182d |*Chem. Mater.* 2011, 23, 3676–3684

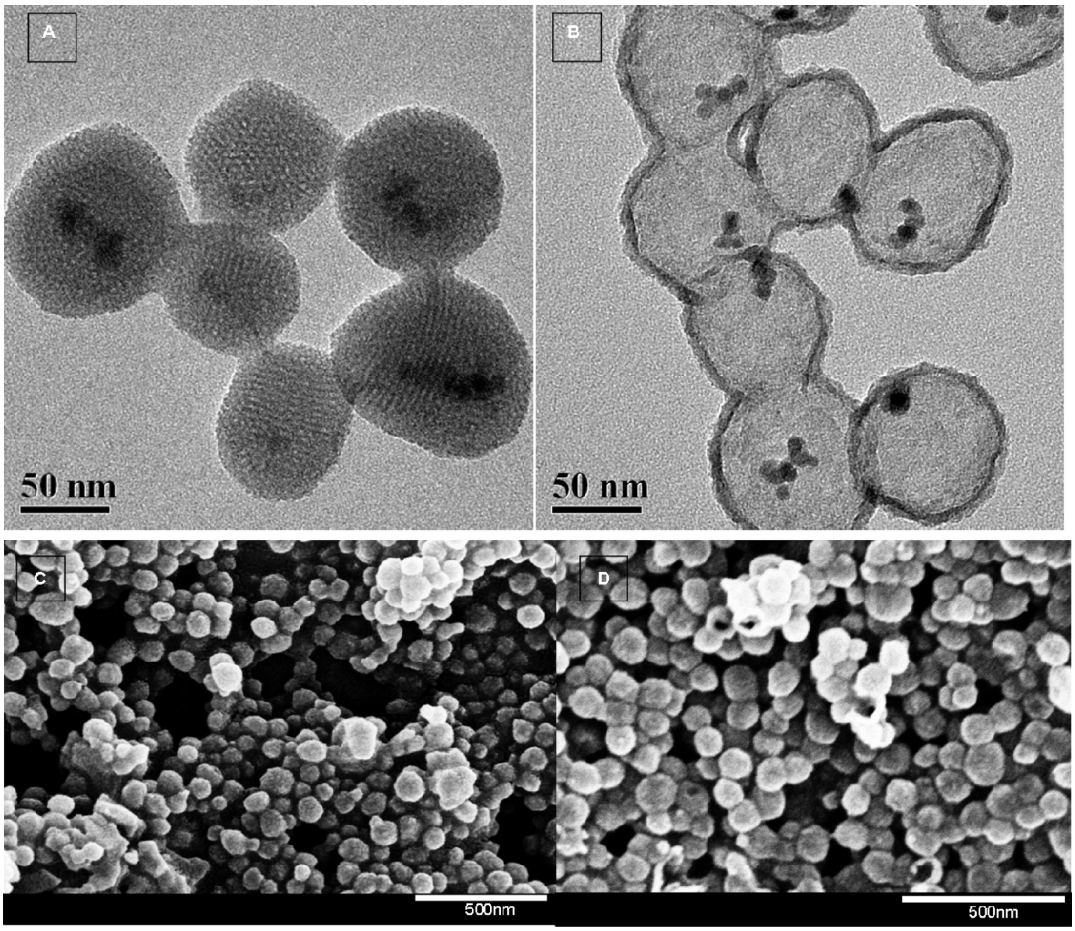

Figure 1. TEM images of Fe_3O_4@SiO_2 core−shell NCs (A), YS-60 (B), and SEM images of Fe_3O_4@SiO_2 core−shell NCs (C) and YS-60 (D).

of yolk−shell NCs is outlined in Scheme 1. The NCs with magnetic cores and mesoporous shells were first synthesized on the basis of a reported method.[50,51] The obtained Fe_3O_4@SiO_2 core−shell NCs have an average particle size of 100 nm and highly ordered hexagonal arranged mesopores in the shells as shown in panel (A) of Figure 1. After addition of 1,2-bis-(trimethoxysilyl)ethane (BTME) into the above synthetic medium, it is interesting to observe that Fe_3O_4@SiO_2 core−shell NCs have completely transformed into the yolk−shell NCs (Figure 1B) after 60 min (this sample was denoted as YS-60, where YS is the abbreviation of yolk−shell and 60 refers to the minutes after the addition of BTME). Uniform and nearly monodisperse yolk−shell NCs with an average particle size of 100 nm and shell thickness of 6 nm were obtained. The SEM image shows that YS-60 is composed of highly uniform NPs, and there is no obvious particle size change compared to the original Fe_3O_4@SiO_2 core−shell NCs (Figure 1C and 1D). The N_2 sorption isotherm of YS-60 shows a type IV isotherm and the pore size distribution centered at 2.4 nm (Figure 2A,B), these results suggest that the obtained yolk−shell NCs have mesoporous shells. Compared with the original Fe_3O_4@SiO_2 core−shell NCs, the BET surface area, pore diameter, and pore volume of YS-60 decreased slightly (Table 1). The saturation magnetization curves (Figure 2C) measured at 300 K show no hysteresis loop, which means that the Fe_3O_4@SiO_2 core−shell NCs and YS-60 sample possess superparamagnetism. With an external magnetic field, the NPs of YS-60 could be easily separated from the solution, while without the external magnetic field the NCs can be homogeneously suspended in alcohol solution as shown in panel (D) of Figure 2.

The above characterizations suggest that the evolution from core−shell to yolk−shell NCs occurs after the addition of BTME to the synthetic medium of the Fe_3O_4@SiO_2 core−shell NCs. It is a very interesting phenomenon for the structure transformation from core−shell to yolk−shell because the Fe_3O_4@SiO_2 core−shell NCs can preserve their structure even after reaction for 20 h (Figure S1 of the Supporting Information). In order to understand the formation mechanism of the yolk−shell NCs, samples were taken out at different reaction time after the addition of BTME. The TEM image of the sample YS-5 obtained after the addition of BTME for only 5 min shows that the structural order in the silica shell decreased and some NCs have lost the highly ordered assemble of the mesopores (Figure 3A). The TEM image of YS-15 obtained after the addition of BTME for 15 min shows that some parts of the NCs become hollow (Figure 3B). The TEM characterizations show that the core−shell NCs gradually transfers into yolk−shell NCs as a function of time after the addition of BTME.

The XRD characterization shows that the intensity of the (110) diffraction peak decreases greatly for YS samples compared with the original Fe_3O_4@SiO_2 core−shell NCs (Figure 4A). The (110) diffraction peak almost disappears in the XRD pattern of YS-60. The XRD and TEM results suggest the gradual destruction of the ordered mesoporous structure in the

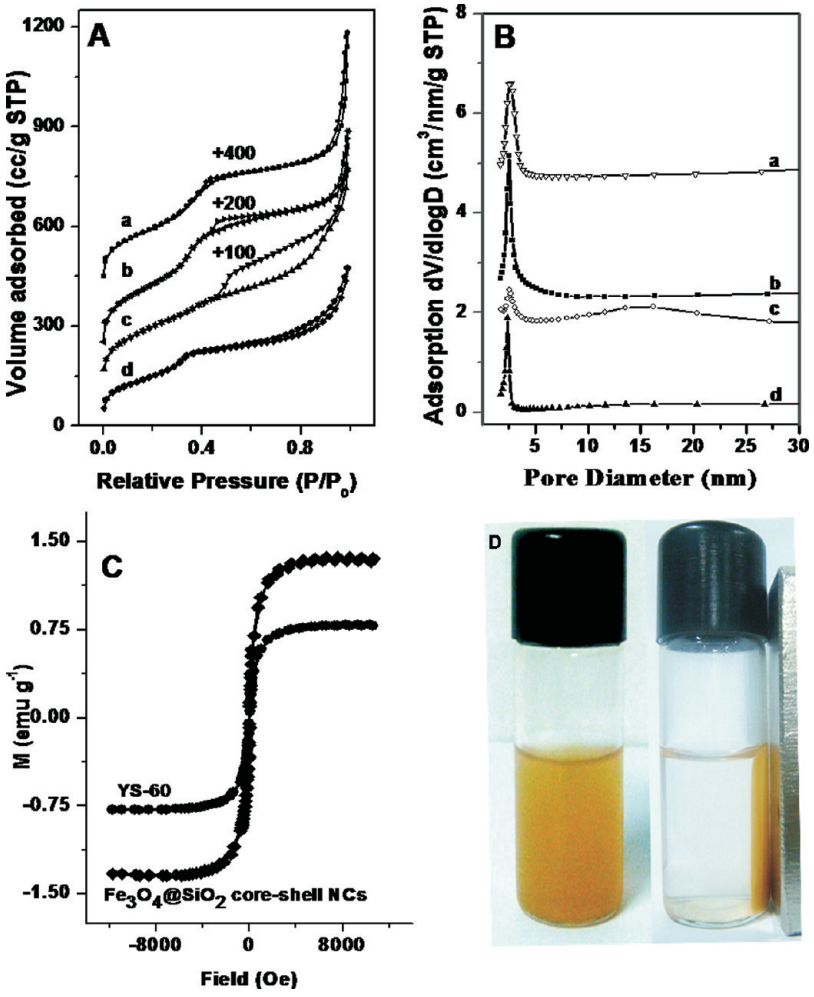

Figure 2. Nitrogen sorption isotherms (A), BJH pore size distribution curves (B) of the samples Fe_3O_4@SiO_2 core−shell NCs (a), YS-5 (b), YS-15 (c), and YS-60 (d); magnetization curves of Fe_3O_4@SiO_2 core−shell NCs and YS-60 at 300 K (C); and the photos of the YS-60 separated from the solution with a magnet (right) and homogeneously suspended in alcohol easily (left) (D). The isotherm pattern for a, b, and c is upshifted for 400, 200, and 100 cm^3g^{-1} respectively.

Table 1. Physicochemical Properties of Core−Shell and Yolk−Shell Materials

sample	S_{BET}[a] ($m^2\ g^{-1}$)	D_{BJH}[b] (nm)	V_t[c] ($cm^3\ g^{-1}$)
Fe_3O_4@SiO_2 core−shell NCs	714	2.7	1.21
YS-5	745	2.5	0.95
YS-15	754	2.5	1.03
YS-60	558	2.4	0.73
YS-60-FC4	592	2.2	1.29
Au@SiO_2 core−shell NCs	634	1.9	0.57
YS-Au-FC4	710	2.0	0.91

[a] S_{BET} is the BET specific surface area. [b] D_{BJH} is BJH pore diameter calculated by the adsorption branches of the nitrogen sorption isotherms. [c] V_t is the total pore volume determined at the relative pressure P/P_0 of 0.99.

silica shells of the Fe_3O_4@SiO_2 core−shell NCs as a function of time after the addition of BTME.

The N_2 sorption isotherms of YS samples summarized in panel (A) of Figure 2 show that all materials have type IV isotherm patterns similar to the original Fe_3O_4@SiO_2 core−shell NCs. A H3 hysteresis loop at relative pressure of $0.45 < P/P_0 < 0.8$ appears in the isotherm pattern of YS-5 and YS-15. Combined with the TEM results, this H3 hysteresis loop is from the void defects in the mesoporous shells and the hollow interior, which were formed during the dissolution process of the silica shells.[52] The physical parameters for all YS samples are summarized in Table 1. The BET surface areas remain almost the same as Fe_3O_4@SiO_2 core−shell NCs for YS-5 and YS-15, but an obvious reduction of the BET surface area was observed for YS-60, which is due to the thin shells (6 nm). The pores in the shells are not directly open to the hollow interior as evidenced from the disappearance of such H3 hysteresis loop in the N_2 sorption isotherm of YS-60 sample. The combined results of TEM, XRD, and N_2 sorption isotherms suggest that the gradual destruction of the mesoporous silica shells and formation of the mesoporous organosilica shells happen after the addition of BTME, and the whole process takes only 60 min.

YS-60-FC4 was prepared in a similar method to YS-60 but using a mixture of CTAB and FC4 as surfactants. The TEM image (Figure S4 of the Supporting Information) clearly shows that YS-60-FC4 has a similar yolk−shell nanostructure

dx.doi.org/10.1021/cm201182d |*Chem. Mater.* 2011, 23, 3676–3684

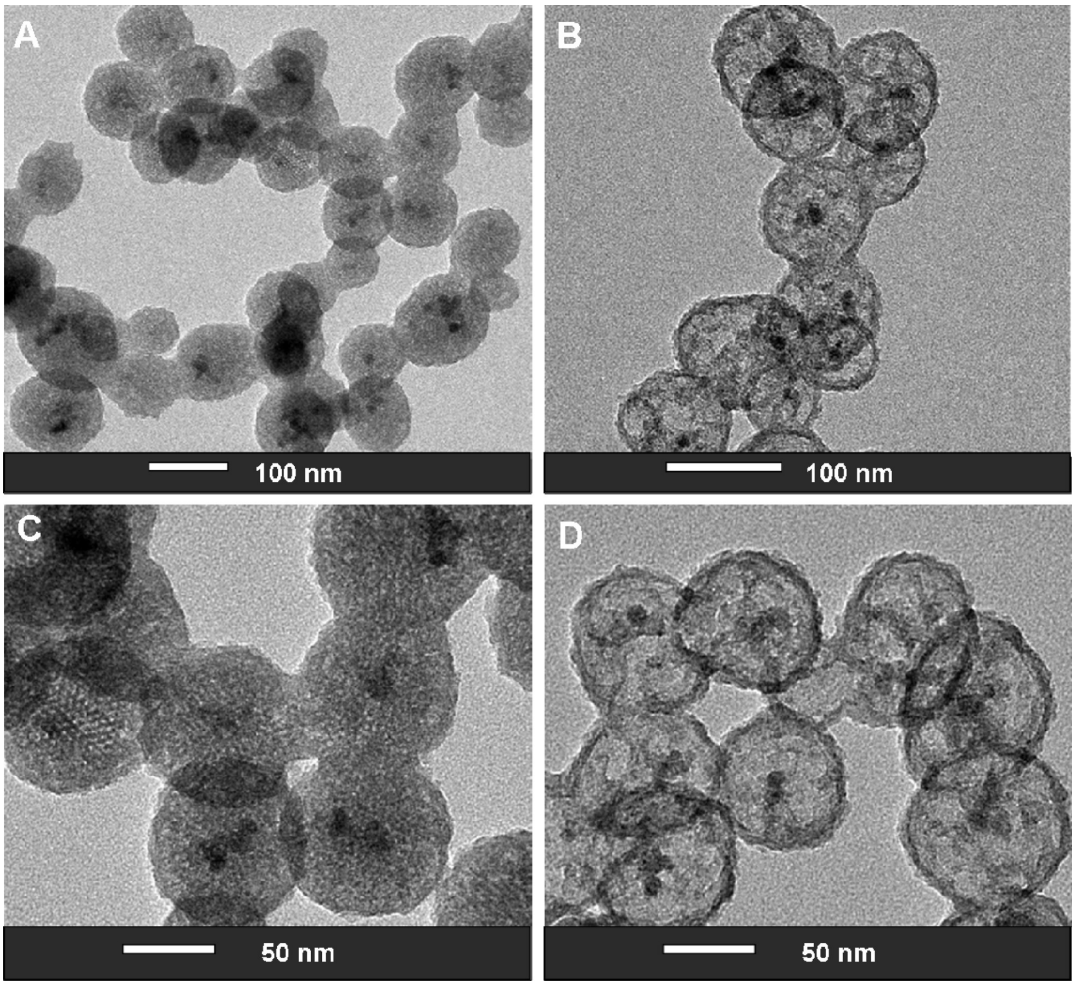

Figure 3. TEM images of YS-5 (A, C) and YS-15 (B, D).

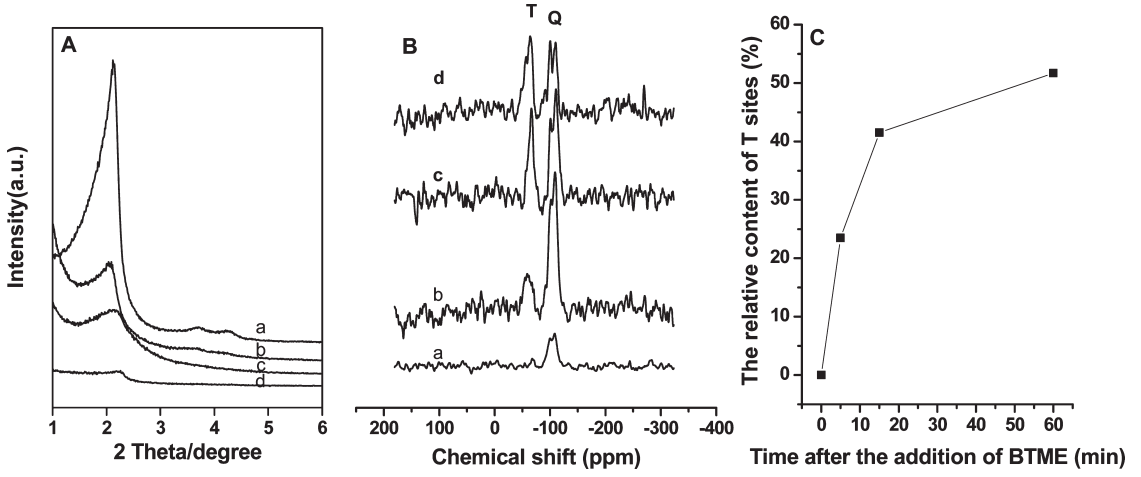

Figure 4. X-ray diffraction patterns (A), ^{29}Si NMR spectra (B) of the samples Fe_3O_4@SiO_2 core−shell NCs (a), YS-5 (b), YS-15 (c), and YS-60 (d), and the relative content of T sites (%) obtained from the ^{29}Si NMR spectra as a function of time after the addition of BTME (C). For ^{29}Si NMR spectroscopy, the samples are characterized after etching the Fe_3O_4 nanoparticles by acid solution.

to YS-60. FC4 and CTAB act as templates for the formation of mesoporous organosilica shells. As a result, YS-60-FC4 has a thicker (13 nm) and porous shell, higher surface area, and larger pore volume than YS-60 (Figure S4 of the Supporting Information and Table 1). Moreover, YS-60-FC4 exhibits a H3 hysteresis loop in its N_2 sorption isotherm, suggesting that the pores in the shell are directly open to the hollow interior.[53] The above results suggest that the porous structure in the shell

dx.doi.org/10.1021/cm201182d |*Chem. Mater.* 2011, 23, 3676–3684

Scheme 2. Illustration of the Evolution Procedure from Core−Shell NCs to Yolk−Shell NCs by the Organosilane-Assisted Etching Process

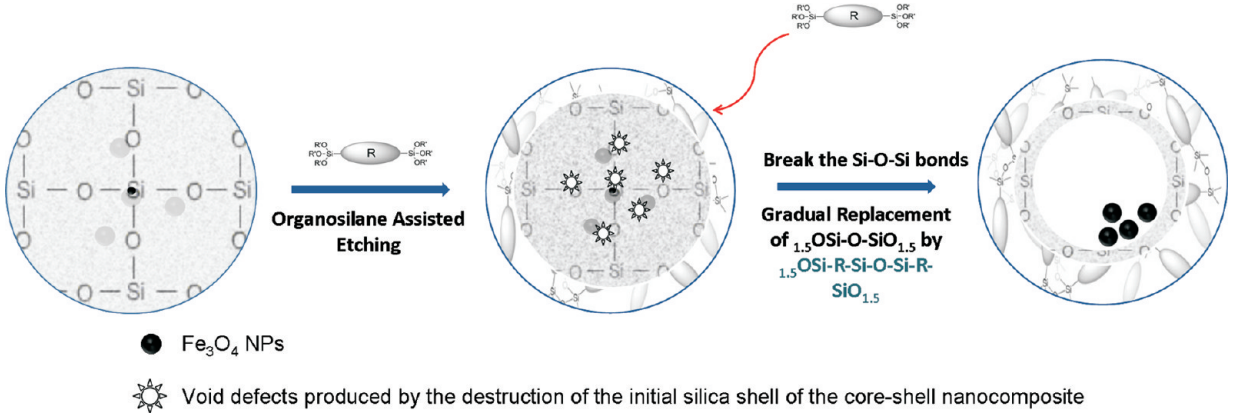

of the yolk−shell NCs could be easily tuned with the aid of different kinds of surfactants.

3.2. Possible Mechanism. For understanding the formation mechanism of the yolk−shell NCs, the chemical compositions of the yolk−shell samples during the structural evolution process were characterized by FT-IR (Figure S2 of the Supporting Information) and ^{29}Si NMR spectroscopy (Figure 4B). In the FT-IR spectra of all the YS-n (n = 5, 15, 60) samples, the appearance of the band at 1407 cm^{-1} and the bands between 2800 and 3000 cm^{-1} assigned to the C−H vibration and stretching vibrations respectively show the incorporation of ethylene groups in the samples due to the condensation of BTME.[54] For Fe_3O_4@SiO_2 core−shell NCs, the typical C−H characteristic peaks cannot be observed, and this result is consistent with the ^{29}Si NMR results that only signals in the range from −90 to −110 ppm assigned to Q sites were observed in the ^{29}Si NMR spectrum of Fe_3O_4@SiO_2 core−shell NCs.[55] The signals attributed to T silicon sites in the range from −45 to −85 ppm were observed for all the YS-n (n = 5, 15, 60) samples, suggesting the formation of organosilica species by condensation of BTME. On the basis of the integration of the peak areas, the T/(T + Q) is 23.5, 41.5, and 51.7% for YS-5, YS-15, and YS-60, respectively (Figure 4C). The T/(T + Q) can reach to 23.5% after the addition of BTME for only 5 min, suggesting fast condensation of the added BTME around the Fe_3O_4@SiO_2 core−shell NCs. ^{29}Si NMR characterization further confirms the gradual replacement of $_{1.5}$OSi−O−$SiO_{1.5}$ species by $_{1.5}$OSi−R−Si−O−Si−R−$SiO_{1.5}$ (R = CH_2CH_2, C_6H_4) species during the structural evolution process. It is notable that 1,4-bis(triethoxysilyl)benzene (BTEB) can also induce the structural evolution from the core−shell to the yolk−shell NCs in a similar way to BTME except that longer reaction time (3 h) was needed (Figure S3A of the Supporting Information). When TMOS and TEOS were used in place of BTME, the core−shell NCs were obtained, and no structural evolution occurred (Figure S3B,C of the Supporting Information).

On the basis of the above results, it can be deduced that the condensation of the organosilane precursors and the dissolution of the silica shells contribute to the formation of the yolk−shell NCs. The possible formation process of the yolk−shell NCs is illustrated in Scheme 2. First, the Fe_3O_4@SiO_2 core−shell mesoporous NCs were formed. TEOS hydrolyzed and condensed incompletely because of the short reaction time (2 h), as proven by the relatively low Q^4/Q^3 ratio (1.42) from the ^{29}Si NMR characterization.[56] This leads to the highly disordered and discontinuous interconnection of the Si−O−Si bonds. After the addition of organosilane precursors such as BTME, the hydrolysis and condensation balance of silica species in the system was broken, and the hydrolysis of Si−O−Si bonds was preferred. The organosilica species deposited on the surface of the core−shell NCs and formed a protective layer, which could prevent the hydrolysis of the Si−O−Si bonds near the outer surface of the core−shell NCs.[11,13,21,22,49,57−60] Therefore, the selective dissolution of the Si−O−Si bonds starts from the inside silica shells of the core−shell NCs. During the structure transformation process, new organosilica species may generated via silica hydrolysis and further condensation with organisilane compounds that stay inside of the protected silica shell, and the yolk−shell NCs with functionalized shell are formed finally.

3.3. Synthesis and Catalytic Performance of Yolk−Shell NCs with Au Cores. Furthermore, this method is very general and can be extended to the synthesis of other metal or metal oxide based yolk−shell NCs. Panels (A) and (B) of Figure 5 illustrate the TEM images of the Au@SiO_2 core−shell and yolk−shell NCs (denoted YS-Au-FC4) with 6 nm Au cores and shell thickness of 23 nm. Highly uniform yolk−shell nanospheres with particle size of 140 nm (Figure 5C) were obtained by the addition of BTME into the synthetic medium of the Au@SiO_2 core−shell NCs under optimized conditions. The SEM image of YS-Au-FC4 sample broken by grinding during SEM sample preparation[61] clearly shows the hollow structures (Figure 5D). The BET surface area, pore diameter, and pore volume of YS-Au-FC4 increased slightly compared with the original Au@SiO_2 core−shell NCs (Table 1 and Figure S5 of the Supporting Information). Similar to YS-60-FC4, the existence of H3 hysteresis loop was observed in the N_2 sorption isotherm, suggesting that the pores in the shell are directly open to the hollow interior.[53] For YS-Au-FC4, the slight increase of BET surface area is probably due to the thick, porous shell and the open pores in the shell (Figure S6 of the Supporting Information). There is no obvious size enlargement of the Au NPs during the structure evolution process (Figure 5A,B). Generally, it is difficult to prepare and assemble the yolk−shell NCs with metal NPs cores smaller than 10 nm.[62] Our method

dx.doi.org/10.1021/cm201182d |Chem. Mater. 2011, 23, 3676–3684

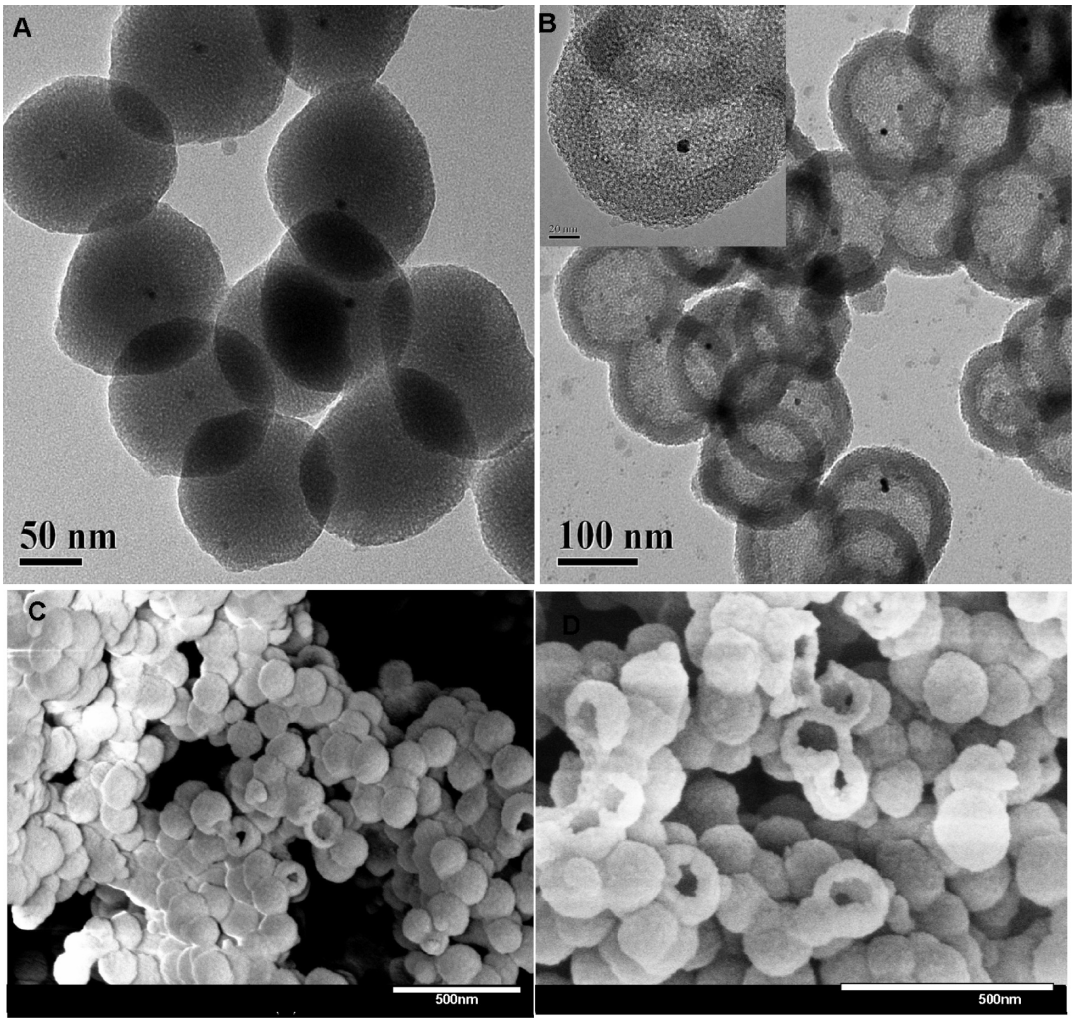

Figure 5. TEM images of $Au@SiO_2$ core−shell NCs (A), YS-Au-FC4 (B), SEM images of YS-Au-FC4 (C), and YS-Au-FC4 sample broken by grinding during SEM sample preparation (D).

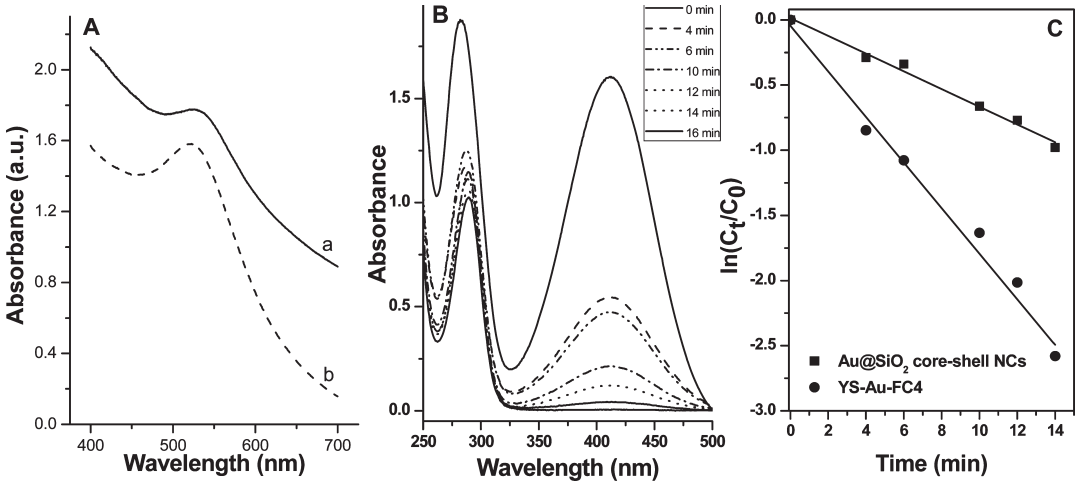

Figure 6. UV−vis spectra (A) of YS-Au-FC4 sample (a) and oleylamine-modified Au NPs (b), time-dependent UV−vis spectral changes of the reaction mixture catalyzed by YS-Au-FC4 (B), and plots of $\ln(C_t/C_0)$ versus time and the rate constants (k_{CS} and k_{YS}) for $Au@SiO_2$ core−shell NCs and YS-Au-FC4, respectively (C).

can easily fabricate yolk−shell NCs with 6 nm Au as moveable cores. The cores of the yolk−shell NCs are believed to be free to move, and in the dry environment of TEM characterization, the cores tend to stick to the walls as a result of the attractive capillary

dx.doi.org/10.1021/cm201182d |*Chem. Mater.* 2011, 23, 3676–3684

force between their surfaces. UV−vis spectra show that the maximum adsorption peak of YS-Au-FC4 (526 nm) exhibits 5 nm red shift compared with that of oleylamine-modified Au NPs (521 nm, Figure 6A). The variation of maximum adsorption peaks is due to the changes of the local refractive index of the surrounding medium.[63]

The catalytic performance of Au@SiO_2 core−shell NCs and YS-Au-FC4 were tested in the catalytic reduction of *o*-nitroaniline (*o*-NA) with $NaBH_4$. The reaction was monitored by taking a small portion of the reaction mixture at specified time. A typical change of the UV−vis absorption during the reaction was shown in panel (B) of Figure 6. The UV−vis peaks at 412 and 282 nm are characteristic of *o*-NA.[19] As the reaction proceeded, the peak at 412 nm disappeared, whereas the 282 nm peak shifted to 289 nm within 16 min for YS-Au-FC4 catalyst. The ratio of C_t and C_0, where C_t is the concentration at time t and C_0 is the initial concentration, was measured from the relative intensity ratio of the respective absorbance, A_t/A_0, at 412 nm. The linear relationship of $\ln(C_t/C_0)$ versus time was observed for both of the catalysts, indicating that the reactions follow first-order kinetics. The observed rate constant k_{CS} = 0.068 min^{-1} and k_{YS} = 0.178 min^{-1}, respectively, for Au@SiO_2 core−shell NCs, and YS-Au-FC4 was estimated directly from the slope of the straight line in panel (C) of Figure 6, which means that the YS-Au-FC4 catalyst shows a much higher catalytic activity than Au@SiO_2 core−shell NCs because of the relatively small mass transport resistance in the shells and much more accessible active sites of the cores from the unique yolk−shell nanostructure. The YS-Au-FC4 catalyst synthesized by our method showed similar catalytic activity to other yolk−shell type gold catalysts in this reaction.[19,62]

4. CONCLUSIONS

In summary, we have developed a novel, general, and rapid one-pot strategy to fabricate yolk−shell nanostructured materials with tailored compositions of the cores and shells. Through the organosilane precursor-assisted etching process, the core−shell nanospheres could be eventually transferred into yolk−shell NCs with Fe_3O_4 (or Au) cores and mesoporous organic−inorganic hybrid silica shells. The yolk−shell NCs with Au cores show high activity in the catalytic reduction of *o*-nitroaniline (*o*-NA). It can be envisioned that yolk−shell NCs with other monometal (such as Pt, Pd, Ag), bimetal, and alloy NPs as cores and variable compositions of mesoporous shells could be synthesized through the current method. The functionalized yolk−shell materials such as those developed in this work with novel properties can have a variety of potential applications, such as confined nanoreactors, drug/gene delivery systems, and building blocks of photonic crystals.

■ ASSOCIATED CONTENT

Supporting Information. FT-IR and TEM images. This material is available free of charge via the Internet at http://pubs.acs.org.

■ AUTHOR INFORMATION

Corresponding Author

*E-mail: yangqh@dicp.ac.cn. Tel: 86-411-84379552. Fax: 86-411-84694447. URL: http://www.hmm.dicp.ac.cn.

■ ACKNOWLEDGMENT

The authors thank the National Basic Research Program of China (2009CB623503) and the National Natural Science Foundation of China (20923001) for financial support.

■ REFERENCES

(1) Lou, X. W.; Wang, Y.; Yuan, C. L.; Lee, J. Y.; Archer, L. A. *Adv. Mater.* **2006**, *18*, 2325.
(2) Zheng, R. B.; Meng, X. W.; Tang, F. Q.; Zhang, L.; Ren, J. *J. Phys. Chem. C* **2009**, *113*, 13065.
(3) Lee, K. T.; Jung, Y. S.; Oh, S. M. *J. Am. Chem. Soc.* **2003**, *125*, 5652.
(4) Cho, M.; Lim, K.; Woo, K. *Chem. Commun.* **2010**, *46*, 5584.
(5) Kim, S. H.; Yin, Y. D.; Alivisatos, A. P.; Somorjai, G. A.; Yates, J. T. *J. Am. Chem. Soc.* **2007**, *129*, 9510.
(6) Roca, M.; Haes, A. J. *J. Am. Chem. Soc.* **2008**, *130*, 14273.
(7) Sun, Y. G.; Wiley, B.; Li, Z. Y.; Xia, Y. N. *J. Am. Chem. Soc.* **2004**, *126*, 9399.
(8) Ren, Y.; Chen, M.; Zhang, Y.; Wu, L. M. *Langmuir* **2010**, *26*, 11391.
(9) Ikeda, S.; Ishino, S.; Harada, T.; Okamoto, N.; Sakata, T.; Mori, H.; Kuwabata, S.; Torimoto, T.; Matsumura, M. *Angew. Chem., Int. Ed.* **2006**, *45*, 7063.
(10) Park, J. C.; Lee, H. J.; Kim, J. Y.; Park, K. H.; Song, H. *J. Phys. Chem. C* **2010**, *114*, 6381.
(11) Zhang, Q.; Zhang, T. R.; Ge, J. P.; Yin, Y. D. *Nano Lett.* **2008**, *8*, 2867.
(12) Güttel, R.; Paul, M.; Schüth, F. *Catal: Sci. Technol.* **2011**, *1*, 65.
(13) Chen, Y.; Chen, H. R.; Zeng, D. P.; Tian, Y. B.; Chen, F.; Feng, J. W.; Shi, J. L. *ACS Nano* **2010**, *4*, 6001.
(14) Gao, J. H.; Liang, G. L.; Cheung, J. S.; Pan, Y.; Kuang, Y.; Zhao, F.; Zhang, B.; Zhang, X. X.; Wu, E. X.; Xu, B. *J. Am. Chem. Soc.* **2008**, *130*, 11828.
(15) Gao, J. H.; Liang, G. L.; Zhang, B.; Kuang, Y.; Zhang, X. X.; Xu, B. *J. Am. Chem. Soc.* **2007**, *129*, 1428.
(16) Arnal, P. M.; Comotti, M.; Schüth, F. *Angew. Chem., Int. Ed.* **2006**, *45*, 8224.
(17) Güttel, R.; Paul, M.; Schüth, F. *Chem. Commun.* **2010**, *46*, 895.
(18) Park, J. C.; Bang, J. U.; Lee, J.; Ko, C. H.; Song, H. *J. Mater. Chem.* **2010**, *20*, 1239.
(19) Lee, J.; Park, J. C.; Bang, J. U.; Song, H. *Chem. Mater.* **2008**, *20*, 5839.
(20) Lee, J.; Park, J. C.; Song, H. *Adv. Mater.* **2008**, *20*, 1523.
(21) Chen, Y.; Chen, H. R.; Guo, L. M.; He, Q. J.; Chen, F.; Zhou, J.; Feng, J. W.; Shi, J. L. *Acs Nano* **2010**, *4*, 529.
(22) Zhao, W. R.; Chen, H. R.; Li, Y. S.; Li, L.; Lang, M.; Shi, J. L. *Adv. Funct. Mater.* **2008**, *18*, 2780.
(23) Liu, J.; Qiao, S. Z.; Hartono, S. B.; Lu, G. Q. *Angew. Chem., Int. Ed.* **2010**, *49*, 4981.
(24) Zhu, Y. F; Ikoma, T.; Hanagata, N.; Kaskel, S. *Small* **2010**, *6*, 471.
(25) Lou, X. W.; Archer, L. A.; Yang, Z. C. *Adv. Mater.* **2008**, *20*, 3987.
(26) Guerrero-Martínez, A.; Pérez-Juste, J.; Liz-Marzán, L. M. *Adv. Mater.* **2010**, *22*, 1182.
(27) Shylesh, S.; Schunemann, V.; Thiel, W. R. *Angew. Chem., Int. Ed.* **2010**, *49*, 3428.
(28) Liu, J.; Liu, F.; Gao, K.; Wu, J. S.; Xue, D. F. *J. Mater. Chem.* **2009**, *19*, 6073.
(29) Liu, J.; Qiao, S. Z.; Hu, Q. H.; Max, Lu, G. Q. *Small* **2011**, *7*, 425.
(30) Wu, X. J.; Xu, D. S. *Adv. Mater.* **2010**, *22*, 1516.
(31) Wu, X. J.; Xu, D. S. *J. Am. Chem. Soc.* **2009**, *131*, 2774.
(32) Cheng, D. M.; Zhou, X. D.; Xia, H. B.; Chan, H. S. O. *Chem. Mater.* **2005**, *17*, 3578.
(33) Yin, Y. D.; Rioux, R. M.; Erdonmez, C. K.; Hughes, S.; Somorjai, G. A.; Alivisatos, A. P. *Science* **2004**, *304*, 711.

(34) Chen, H. M.; Liu, R. S.; Asakura, K.; Lee, J. F.; Jang, L. Y.; Hu, S. F. *J. Phys. Chem. B* **2006**, *110*, 19162.
(35) Vasquez, Y.; Sra, A. K.; Schaak, R. E. *J. Am. Chem. Soc.* **2005**, *127*, 12504.
(36) Lou, X. W.; Yuan, C. L.; Archer, L. A. *Adv. Mater.* **2007**, *19*, 3328.
(37) Li, H. X.; Bian, Z. F.; Zhu, J.; Zhang, D. Q.; Li, G. S.; Huo, Y. N.; Li, H.; Lu, Y. F. *J. Am. Chem. Soc.* **2007**, *129*, 8406.
(38) Kamata, K.; Lu, Y.; Xia, Y. N. *J. Am. Chem. Soc.* **2003**, *125*, 2384.
(39) Kim, M.; Sohn, K.; Na, H. B.; Hyeon, T. *Nano Lett.* **2002**, *2*, 1383.
(40) Xing, S. X.; Tan, L. H.; Chen, T.; Yang, Y. H.; Chen, H. Y. *Chem. Commun.* **2009**, 1653.
(41) Lou, X. W.; Yuan, C. L.; Archer, L. A. *Small* **2007**, *3*, 261.
(42) Chen, D.; Li, L. L.; Tang, F. Q.; Qi, S. O. *Adv. Mater.* **2009**, *21*, 3804.
(43) Yi, D. K.; Lee, S. S.; Papaefthymiou, G. C.; Ying, J. Y. *Chem. Mater.* **2006**, *18*, 614.
(44) Zhang, T. R.; Ge, J. P.; Hu, Y. X.; Zhang, Q.; Aloni, S.; Yin, Y. D. *Angew. Chem., Int. Ed.* **2008**, *47*, 5806.
(45) Zhu, Y.; Kockrick, E.; Ikoma, T.; Hanagata, N.; Kaskel, S. *Chem. Mater.* **2009**, *21*, 2547.
(46) Zhang, X. F.; Clime, L.; Roberge, H.; Normandin, F.; Yahia, L. H.; Sacher, E.; Veres, T. *J. Phys. Chem. C* **2011**, *115*, 1436.
(47) Zhu, J. X.; Sun, T.; Hng, H. H.; Ma, J.; Boey, F. Y. C.; Lou, X. W.; Zhang, H.; Xue, C.; Chen, H. Y.; Yan, Q. Y. *Chem. Mater.* **2009**, *21*, 3848.
(48) Teng, Z. G.; Li, J.; Yan, F.; Zhao, R.; Yang, W. S. *J. Mater. Chem.* **2009**, *19*, 1811.
(49) Peng, S.; Lee, Y. M.; Wang, C.; Yin, H. F.; Dai, S.; Sun, S. H. *Nano Res.* **2009**, *2*, 583.
(50) Fan, H. Y.; Yang, K.; Boye, D. M.; Sigmon, T.; Malloy, K. J.; Xu, H. F.; Lopez, G. P.; Brinker, C. J. *Science* **2004**, *304*, 567.
(51) Kim, J.; Lee, J. E.; Lee, J.; Yu, J. H.; Kim, B. C.; An, K.; Hwang, Y.; Shin, C. H.; Park, J. G.; Hyeon, T. *J. Am. Chem. Soc.* **2006**, *128*, 688.
(52) Liu, J.; Yang, Q. H.; Zhang, L.; Jiang, D. M.; Shi, X.; Yang, J.; Zhong, H.; Li, C. *Adv. Funct. Mater.* **2007**, *17*, 569.
(53) Wang, J. G.; Li, F.; Zhou, H. J.; Sun, P. C.; Ding, D. T.; Chen, T. H. *Chem. Mater.* **2009**, *21*, 612.
(54) Zhang, L.; Liu, J.; Yang, J.; Yang, Q. H.; Li, C. *Microporous Mesoporous Mater.* **2008**, *109*, 172.
(55) Liu, X.; Wang, P. Y.; Yang, Y.; Wang, P.; Yang, Q. H. *Chem. Asian J.* **2010**, *5*, 1232.
(56) Liu, X.; Wang, P. Y.; Zhang, L.; Yang, J.; Li, C.; Yang, Q. H. *Chem.—Eur. J.* **2010**, *16*, 12727.
(57) Hu, Y. X.; Zhang., Q.; Goebl, J.; Zhang, T. R.; Yin, Y. D. *Phys. Chem. Chem. Phys.* **2010**, *12*, 11836.
(58) Zhang, Q.; Ge, J. P.; Goebl, J.; Hu, Y. X.; Sun, Y. G.; Yin, Y. D. *Adv. Mater.* **2010**, *22*, 1905.
(59) Zhang, Q.; Lee, I.; Ge, J. P.; Zaera, F.; Yin, Y. D. *Adv. Funct. Mater.* **2010**, *20*, 2201.
(60) Alexander, G. B.; Heston, W. M.; Iler, R. K. *J. Phys. Chem.* **1954**, *58*, 453.
(61) Li, J.; Liu, J.; Wang, D. H.; Guo, R. S.; Li, X. L.; Qi, W. *Langmuir* **2010**, *26*, 12267.
(62) Tan, L. F.; Chen, D.; Liu, H. Y.; Tang, F. Q. *Adv. Mater.* **2010**, *22*, 4885.
(63) LizMarzan, L. M.; Giersig, M.; Mulvaney, P. *Langmuir* **1996**, *12*, 4329.